https://doi.org/10.1590/jatm.v18.1450

ORIGINAL PAPER

Modeling and Integrated Control Design for Folding-Wing Aircraft during Morphing Process

Zexin Wang[1,*]

1.Beijing Institute of Control Engineering – Research and Development Center – Beijing – China.

*Corresponding author: wangzx@buaa.edu.cn

ABSTRACT

This paper proposes a novel integrated robust control framework tailored for folding-wing aircraft during large-angle morphing maneuvers. The morphing process induces severe nonlinearities, strong coupling between wing kinematics and vehicle dynamics, and significant time-varying shifts in the center of gravity and aerodynamic characteristics, posing substantial challenges to flight stability. To address these issues, a two-time-scale hybrid control architecture is developed: a robust sliding mode controller (SMC) governs the fast inner-loop attitude dynamics to counteract model uncertainties and disturbances, while a well-tuned proportional-integral-derivative (PID) controller manages the slower outer-loop trajectory variables, such as altitude and velocity. A high-fidelity multi-body dynamic model is derived from first principles using Newtonian mechanics, fully accounting for morphing-induced inertial and aerodynamic variations. Extensive closed-loop simulations validate the approach, achieving stable transitions with altitude errors within ± 1.5 m, velocity errors below ± 1.8 $m \cdot s^{-1}$, and settling times under 50 seconds – even under ± 20% perturbations in aerodynamic coefficients. To the best of the author' knowledge, this is the first implementation of a hybrid SMC–PID strategy specifically designed for large-scale rigid-body wing reconfiguration, offering a practical and theoretically grounded pathway toward deployable morphing aircraft systems.

Keywords: Folding-wing aircraft; Robust control; Sliding mode control; Morphing aircraft.

INTRODUCTION

Morphing aircraft can adaptively alter their aerodynamic configuration to enhance flight performance across diverse flight phases and mission profiles (Bai *et al.* 2020; Umar *et al.* 2025; Dai *et al.* 2021; Liu *et al.* 2019; Nie and Zhou 2021; Peng *et al.* 2019; Takarics *et al.* 2020; Zhen *et al.* 2017; Zhu *et al.* 2017). These aircraft offer multi-objective adaptability, resulting in a wider flight envelope and higher combat effectiveness compared to conventional fixed-wing aircraft (Moorhouse *et al.* 2006). Recent research has explored various morphing strategies and control co-design approaches, such as the simultaneous stochastic redesign of autopilot, powerplant, and tail surfaces for performance enhancement (Özgür *et al.* 2025; Yesilbas *et al.* 2025), active rotor morphing for helicopter control energy savings (Oktay and Sultan 2014), and minimum-energy control for tiltrotor aircraft (Oktay 2014). Optimization techniques such as simultaneous perturbation stochastic approximation have also been employed to co-design morphing mechanisms and proportional-integral-derivative (PID) controllers for quadcopters (Kose *et al.* 2023) and *vertical take-off and landing* (VTOL) *unmanned aerial vehicles (*UAVs) (Kocamer *et al.* 2025).

This paper focuses on the modeling and control design for folding-wing aircraft, a specific class of morphing aircraft in which the wing-folding process involves significant rigid-body motion of the wing structure. As wing configurations and aerodynamics

Received: Feb. 07, 2026 | **Accepted:** May 14, 2026
Peer Review History: Single Blind Peer Review.
Section editor: Luiz Martins-Filho

vary on a large scale, substantial variations in the dynamic response and kinetic parameters occur. In addition, the folding-wing aircraft takes a long time to reach a new equilibrium flight state without active control. Consequently, the flying qualities and flight safety of the folding-wing aircraft may deteriorate significantly. Therefore, a robust flight controller is needed to guarantee stability and smoothness during the morphing process. During the wing-folding process, the aircraft's configuration and aerodynamics undergo large-scale variations, leading to substantial changes in kinetic parameters. Furthermore, the folding-wing aircraft requires considerable time to reach a new equilibrium flight state without active control. This can lead to significant deterioration in flying qualities and safety during the morphing process, necessitating a robust flight controller to ensure stability and a smooth transition.

Current research on controllers designed to ensure a smooth and stable wing transition is primarily based on gain-scheduling control methods, in which controller parameters are varied according to the changing aerodynamics and structural properties during the morphing process (Apkarian *et al.* 1995; Wu *et al.* 2013). However, this approach cannot guarantee global stability and robustness due to imprecise aerodynamic modeling in the transition phase and the strong coupling between mass distribution and wing configurations (Yue and Wang 2013). Similarly, model predictive control (MPC), while effective for constrained optimization, faces substantial computational demands when applied to the high-dimensional, nonlinear models required for folding-wing aircraft.

Given these challenges associated with model uncertainties, strong parameter variations, and the lack of global stability guarantees in existing gain-scheduling- or MPC-based approaches, this paper proposes a practically implementable, two-loop integrated robust flight controller that uniquely leverages the complementary strengths of sliding mode control and PID control. The key novelty lies in the explicit separation of control responsibilities based on time-scale dynamics and model fidelity: the sliding mode controller (SMC) handles the highly uncertain, fast-changing inner-loop dynamics during morphing, while PID regulates the slower, more predictable outer-loop flight-path variables. The field has seen advancements in diverse morphing strategies (Apkarian *et al.* 1995; Peng *et al.* 2019) and robust control methods for handling parameter variations (Bai *et al.* 2020; Nie and Zhou 2021; Zhen *et al.* 2017). However, a control strategy explicitly designed for the two-time-scale challenge of large-angle, rigid-body morphing remains underexplored. This work addresses this gap by proposing a novel hybrid SMC-PID architecture. Its core novelty lies in the explicit, principle-based allocation of robust SMC to the fast, uncertain inner-loop dynamics and stable PID to the slower outer loop, ensuring smooth and stable transitions despite significant model uncertainties arising from the morphing process. In addition, an application is presented for a hybrid robust control framework specifically tailored to the longitudinal dynamics of folding-wing aircraft undergoing large-angle wing reconfiguration.

Longitudinal model of the folding-wing aircraft

Modeling by Newtonian mechanics

The folding-wing aircraft is a multibody dynamic system during the wing-folding process. Newtonian mechanics is used to model the multibody dynamics of this aircraft. The wing of the folding-wing aircraft consists of an inner wing and an outer wing. The inner wing is fixed on the fuselage of the aircraft, and the outer wing can be folded upward around its shaft, which is parallel to the fuselage axis by 60° using an actuator. Its configuration is shown in Fig. 1.

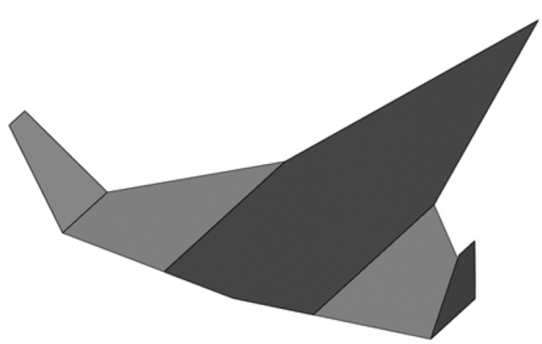

Source: Elaborated by the author.

Figure 1. Configuration of the folding-wing aircraft.

The center of gravity (CG) of the folding-wing aircraft changes along the fuselage axis due to the movement of the outer wing. In this paper, origin of the body coordinate system $o_b x_b y_b z_b$ is set at the CG of the morphing aircraft in the wing fully extended wing configuration, and the ground coordinate system is denoted as $o_g x_g y_g z_g$. The folding-wing aircraft structure can be divided into the fuselage, inner wing, and outer wing, whose CG is expressed as c_i (i =1,..., n), as shown in Fig. 2.

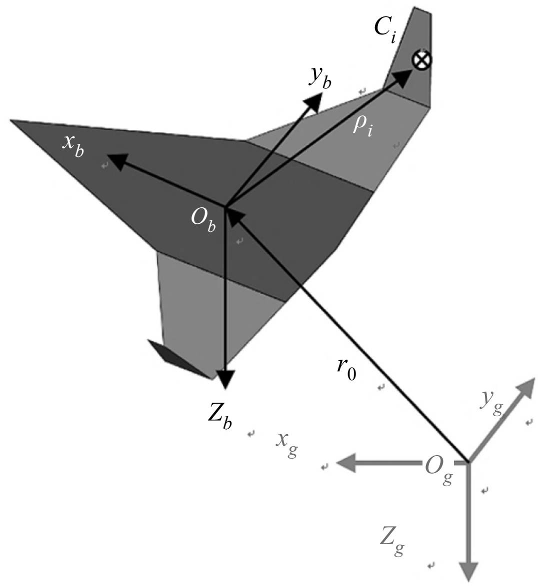

Source: Elaborated by the author.

Figure 2. Coordinate systems.

The momentum $\boldsymbol{p}$ and moment of momentum $\boldsymbol{H}$ in the body coordinate system $o_b x_b y_b z_b$ can be expressed as:

$$\begin{cases} \boldsymbol{p} = m\boldsymbol{V} + \dfrac{\delta \boldsymbol{S}}{\delta t} + \boldsymbol{\omega} \times \boldsymbol{S} \\ \boldsymbol{H} = \boldsymbol{S} \times \boldsymbol{V} + \boldsymbol{I} \cdot \boldsymbol{\omega} + \sum_{i=1}^{n} [\dfrac{1}{m_i} \boldsymbol{S}_i \times \dfrac{\delta \boldsymbol{S}_i}{\delta t} + \boldsymbol{I}_i \cdot \boldsymbol{\omega}_i] \end{cases} \tag{1}$$

where $\boldsymbol{S}$ is the static moment vector, m is the mass of the whole aircraft, m_i represents the mass of each part of the morphing aircraft, and $\boldsymbol{I}$ is the moment of inertia about the centroid of the aircraft, that is:

$$\boldsymbol{I} = \begin{bmatrix} I_x & -I_{xy} & -I_{zx} \\ -I_{xy} & I_y & -I_{yz} \\ -I_{yz} & -I_{yz} & I_z \end{bmatrix} \tag{2}$$

The origin of the body coordinate system does not always locate at the CG of the folding-wing aircraft during the wing-folding process. According to the dynamics of multibody systems (Shabana 2020),

$$\boldsymbol{F} = \dot{\boldsymbol{p}} \tag{3}$$

$$\boldsymbol{M} - \boldsymbol{V} \times \dot{\boldsymbol{S}} = \dot{\boldsymbol{H}} \tag{4}$$

By Eqs. 2 and 3, the dynamic equations of the folding-wing aircraft in vector form can be expressed as:

$$\begin{aligned} \boldsymbol{F} &= m(\frac{\delta \boldsymbol{V}}{\delta t} + \boldsymbol{\omega} \times \boldsymbol{V}) + \frac{\delta \boldsymbol{\omega}}{\delta t} \times \boldsymbol{S} \\ &+ 2\boldsymbol{\omega} \times \frac{\delta \boldsymbol{S}}{\delta t} + \boldsymbol{\omega} \times (\boldsymbol{\omega} \times \boldsymbol{S}) + \frac{\delta^2 \boldsymbol{S}}{\delta t^2} \end{aligned} \tag{5}$$

$$\begin{aligned} \boldsymbol{M} &= \boldsymbol{I} \cdot \frac{\delta \boldsymbol{\omega}}{\delta t} + \frac{\delta \boldsymbol{I}}{\delta t} \cdot \boldsymbol{\omega} + \boldsymbol{\omega} \times (\boldsymbol{I} \cdot \boldsymbol{\omega}) + \boldsymbol{S} \times \frac{\delta \boldsymbol{V}}{\delta t} + \boldsymbol{S} \times (\boldsymbol{\omega} \times \boldsymbol{V}) \\ &+ \sum_{i=1}^{n} \{ \boldsymbol{I}_i \cdot \frac{\delta \boldsymbol{\omega}_i}{\delta t} + \frac{\delta \boldsymbol{I}_i}{\delta t} \cdot \boldsymbol{\omega}_i + \boldsymbol{\omega}_i \times (\boldsymbol{I}_i \cdot \boldsymbol{\omega}_i) \} \\ &+ \sum_{i=1}^{n} \frac{1}{m_i} [\boldsymbol{S}_i \times \frac{\delta^2 \boldsymbol{S}_i}{\delta t^2} + \boldsymbol{\omega} \times (\boldsymbol{S}_i \times \frac{\delta \boldsymbol{S}_i}{\delta t})] \end{aligned} \tag{6}$$

In Eq. 6, $\boldsymbol{F}$ and $\boldsymbol{M}$ are the force and torque vectors acting on the aircraft, ω represents the rotational angular velocity of the body coordinate relative to the ground coordinate, and $\boldsymbol{S}$ is the static moment vector. A detailed list of all symbols and their units is provided in Tables 1 and 2.

Table 1. Roman symbols.

Symbol	Description	Units
α	Angle of attack	rad
α_c	Angle of attack command	rad
α_α	Power of α loop switching gain function	-
α_q	Power of q loop switching gain function	-
β_q	Switching gain	-
δ_e	Elevator deflection	rad
ε	Boundary layer thickness	-
θ	Pitch angle	rad
ω_α	Parameter of α loop switching gain function	-
ω_q	Parameter of q loop switching gain function	-
ω	Angular velocity	$rad \cdot s^{-1}$

Source: Elaborated by the author.

Table 2. Greek symbols.

Symbol	Description	Units
c	Wing chord	m
c_α	Sliding surface slope of α loop	-
c_q	Sliding surface slope of q loop	-
C_L	Lift coefficient	-
C_D	Drag coefficient	-

Continue...

Continuation.

C_M	Pitch moment coefficient	-
C_{L0}	Lift coefficient at aero lift	-
C_{D0}	Drag coefficient at aero lift	-
C_{m0}	Pitch moment coefficient at aero lift	-
$C_{L\alpha}$	Lift coefficient relative to the angle of attack	-
C_{LV}	Lift coefficient relative to the airspeed	-
C_{Lq}	Lift coefficient relative to the pitch rate	-
$C_{L\alpha e}$	Lift coefficient relative to the derivative of the angle of attack	-
$C_{L\delta e}$	Lift coefficient relative to the elevator deflection	-
$C_{D\alpha}$	Drag coefficient relative to the angle of attack	-
C_{DV}	Drag coefficient relative to the airspeed	-
$C_{m\alpha}$	Pitch moment coefficient relative to the angle of attack	-
C_{mV}	Pitch moment coefficient relative to the airspeed	-
D	Aerodynamic drag	N
D_H	Altitude PID derivative gain	rad·s·m^{-1}
D_V	Velocity PID derivative gain	N·s·(m^{-1}·s)
Δf_f	Uncertainty of pitch rate dynamics	-
Δf_s	Uncertainty of α dynamics	-
F	Aerodynamic force	N
g	Gravitational acceleration	m·s^{-2}
H	Moment of momentum	N·m·s
H_c	Altitude command	m
H	Altitude	m
I	Moment of inertia	kg·m^2
I_H	Altitude PID integral gain	Rad·(m·s)$^{-1}$
I_V	Velocity PID integral gain	N·m^{-1}
L	Aerodynamic lift	N
L_q	Bound of pitch rate dynamics uncertainty	-
L_α	Bound of α loop dynamics uncertainty	-
M	Torque	N·m
M_A	Aerodynamic torque	N·m
M_α	Mach number	-
M_T	Thrust torque	N·m
$M_{y\text{-}\delta e}$	Pitch torque in addition to the elevator	Nm
ΔM	Pitch torque uncertainty	Nm
$\Delta M_{\max}$	Pitch torque uncertainty bound	Nm
N	Coefficient of the approximate differentiator	Hz
p	Momentum	N·s
P_H	Altitude PID proportional gain	rad/m
P_V	Velocity PID proportional gain	N·(m^{-1}·s)
q	Pitch rate	rad·s^{-1}
q_c	Pitch rate reference command	rad·s^{-1}
S	Static moment	kg·m
S_*	Static moment component in the axis of the body coordinate	kg·m
S	Laplace operator	-
S_q	Sliding surface of q loop	-
S_α	Sliding surface of α loop	-
T	Thrust	N
T_c	Thrust command	N
V	Airspeed	m·s^{-1}
V_c	Speed command	m·s^{-1}
V_*	Airspeed in the axis of the body coordinate	m·s^{-1}

Source: Elaborated by the author.

Only the longitudinal responses in the wing-folding process are considered. By simplifying Eq. 4,

$$\begin{cases} F_x = m(\dot{V}_x + qV_z) + \dot{q}S_z + q\dot{S}_z \\ F_z = m(\dot{V}_z - qV_x) - q^2 S_z \\ M_y = I_y \dot{q} + \dot{I}_y q + S_z \dot{V}_x + S_z q V_z \end{cases} \tag{7}$$

In Eq. 7, $\dot{V}$ is the airspeed and $\dot{S}$ is the static moment. Their subscripts represent the components of the vectors on each axis of the body coordinate system.

The force and torque on the left side of the equation can be simplified by ignoring the second-order small terms. Consequently, they are expressed as:

$$\begin{cases} F_x = -D\cos\alpha + L\sin\alpha + T\cos\varphi_T - mg\sin\theta \\ F_z = -D\sin\alpha - L\cos\alpha - T\sin\varphi_T + mg\cos\theta \\ M_y = M_A - M_T - S_z g\sin\theta \end{cases} \tag{8}$$

where α is the angle of attack, θ is the pitch angle, φ_T is the angle of engine installation, D,L,T are drag, lift, and thrust, and M_A,M_T are the torques generated by the aerodynamics and thrust.

Longitudinal aerodynamic model

The wing-folding process causes unsteady aerodynamic forces, which are difficult to calculate precisely. Therefore, an engineering approximation of unsteady aerodynamics based on recent research is used.

Yue and Wang (2013) demonstrated that drag, lift, and pitch moment coefficients under different folding angular velocities exhibit only minor deviations from steady-state values and vary approximately linearly with the wing-folding angle. This finding implies that dynamic responses caused by unsteady aerodynamics during wing folding can be reasonably neglected for control design purposes.

Building upon this quasi-steady assumption, the longitudinal aerodynamic coefficients during the wing-folding process are modeled as linear interpolations between the fully extended and fully folded configurations. This approach provides a computationally efficient yet sufficiently accurate representation for control design purposes, expressed as:

$$\begin{cases} C_D = C_{D0} + C_{D\alpha}\alpha + C_{DV}\Delta V / V \\ C_L = C_{L0} + C_{L\alpha}\alpha + C_{LV}\Delta V / V + \\ \qquad C_{Lq} q / (2V/c) + C_{L\dot{\alpha}}\dot{\alpha} / (2V/c) + C_{L\delta_e}\delta_e \\ C_M = C_{m0} + C_{m\alpha}\alpha + C_{mV}\Delta V / V + \\ \qquad C_{mq} q / (2V/c) + C_{m\dot{\alpha}}\dot{\alpha} / (2V/c) + C_{m\delta_e}\delta_e \end{cases} \tag{9}$$

where C_{D0}, C_{L0} and C_{m0} are the drag, lift, and pitch torque coefficients at aero lift, q is the pitch rate, c is the wing chord, and C_{D*}, C_{L*}, C_{m*} ("*" represents the subscripts "α, $\dot{\alpha}$, V, q, δ_e") are the drag, lift, and moment non-dimensional coefficients of each variable, respectively. A detailed list of all symbols and their units is provided in Tables 1 and 2.

Design of the integrated flight controller

The folding-wing aircraft exhibits strongly nonlinear and time-varying behavior during morphing, compounded by model uncertainty arising from the quasi-steady aerodynamic approximation. To address this, an integrated flight control architecture grounded in time-scale separation is introduced – a principle that enables optimal allocation of control effort according to system dynamics and model reliability.

The integrated flight control system is divided into outer loop and inner loop subsystems according to the time-scale separation principle. The inner loop, comprising the angle-of-attack (α) and pitch-rate (q) control channels, operates at a much faster timescale and is subject to significant unmodeled aerodynamic effects. Hence, SMC is employed in this loop to provide guaranteed robustness against bounded uncertainties – a core innovation of the design. In contrast, the outer flight-path loop, which commands altitude and velocity, evolves slowly and is less sensitive to high-frequency morphing-induced disturbances; thus, a well-tuned PID controller suffices and offers simplicity and ease of implementation. This hybrid SMC-PID structure represents a pragmatic yet theoretically sound solution that balances robustness, performance, and engineering feasibility.

In this paper, the integrated control design is analyzed based on a speed- and altitude-holding task. The overall controller structure is shown in Fig. 3.

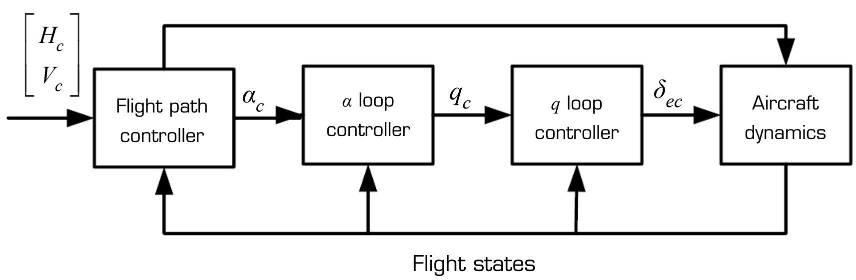

Source: Elaborated by the author.

Figure 3. Overall controller structure.

Sliding mode control design for q loop

The q loop dynamic equation of the folding-wing aircraft can be modeled as the following nonlinear affine system. A detailed list of all symbols and their units is provided in Tables 1 and 2.

$$\begin{cases} \dot{q} = f_f(q,t) + g_f(t)\delta_e(t) \\ y = q \end{cases} \tag{10}$$

where $\delta_e(t)$ is the elevator deflection input, $f_f(q,t)$ is the nonlinear drift term in the pitch-rate dynamics, and $g_f(t)$ is the input gain function for pitch rate. $f_f(q,t)$ and $g_f(t)$ are calculated from the flight states, structure, and aerodynamic parameters of the folding-wing aircraft, and they can be expressed as follows:

$$\begin{cases} f_f(q,t) = \dfrac{1}{I_y}(M_{y-\delta_e} - \dot{I}_y q - S_z \dot{V}_x - S_z q V_z) \\ g_f(t) = \dfrac{C_{M\delta_e}}{I_y} \end{cases} \tag{11}$$

$M_{y-\delta_e}$ stands for the pitch torque generated by the whole aircraft in addition to the elevator. According to the preceding analysis, $M_{y-\delta_e}$ includes the uncertainty of the unsteady aerodynamics, which can be expressed as:

$$M_{y-\delta_e} = \bar{M}_{y-\delta_e} + \Delta M \tag{12}$$

where $\bar{M}_{y-\delta_e}$ is the nominal value of $M_{y-\delta_e}$ and ΔM is the bounded uncertainty (Yue and Wang 2013). It satisfies $|\Delta M| \le \Delta M_{\max}$, where $\Delta M_{\max}$ is a positive constant representing the uncertainty bound.

The integrated control design problem is described as follows. Given a real-time commanded reference profile $y_c(t)$, a sliding mode control law is designed such that the system tracks the reference with bounded error despite modeling uncertainties. Therefore, the main task of the q loop controller is to force the output signal q to track the given reference command q_c. This means the tracking error $e(t) = q(t) - q_c(t)$ should asymptotically approach zero:

$$\lim_{t \to \infty} \|e(t)\| = \lim_{t \to \infty} \|q(t) - q_c(t)\| \to 0, \forall t > 0 \tag{13}$$

The sliding surface is chosen t s_q as:

$$s_q = e + c_q \int edt \tag{14}$$

where c_q is a positive constant, representing the sliding surface slope and determines the convergence rate.

Therefore, the dynamics of the system on the sliding surface are derived as follows.

$$\begin{aligned} \dot{s}_q &= \dot{e} + c_q e \\ &= f_f(q,t) + g_f(t)\delta_e(t) - \dot{q}_c + c_q(q - q_c) \end{aligned} \tag{15}$$

Rewrite the function $f_f(q,t)$ considering the uncertainty:

$$f_f(q,t) = \overline{f}_f(q,t) + \Delta f_f \tag{16}$$

where $\overline{f}_f(q,t)$ is the nominal value of $f_f(q,t)$ and Δf_f is the bounded uncertainty, which meets the following bound (Yue and Wang 2013):

$$|\Delta f_f| < L_q \tag{17}$$

and L_q is a positive bound of the pitch rate dynamics uncertainty:

$$\dot{s}_q = \overline{f}_f(q,t) + \Delta f_f + g_f(t)\delta_e(t) - \dot{q}_c + c_q(q - q_c) \tag{18}$$

Employ the following feedback control law

$$\delta_e = \frac{1}{g_f(t)}\left[-\overline{f}_f(t) - L_q - c_q(q - q_c) + \dot{q}_c - \beta_q \operatorname{sat}(s_q)\right] \tag{19}$$

where β_q is a positive definite switching gain function, designed to dominate uncertainty, and sat$(\cdot)$ is the saturation function defined by:

$$\operatorname{sat}(s_q) = \begin{cases} 1 & s_q > \varepsilon \\ s_q/\varepsilon & |s_q| \le \varepsilon \\ -1 & s_q < -\varepsilon \end{cases} \tag{20}$$

and ε is the boundary layer thickness (a positive constant), which determines chattering reduction.

The last term in Eq. 19 provides robustness against uncertainties through discontinuous switching action, and the other terms represent the equivalent control that cancels nominal dynamics.

This control law consists of continuous and switching components to reduce the amplitude of the switching control. Combined with the saturation function, it mitigates chattering in the closed-loop system (Khalil 2008). The saturation function creates a boundary layer of thickness ε around the sliding surface, within which the control action becomes continuous linear feedback, effectively reducing high-frequency oscillations while maintaining robustness.

To prove that Eq. 14 is asymptotically stable under the control law in Eq. 19, the Lyapunov function is chosen as:

$$V_q = \frac{1}{2} s_q^{\,2} \tag{21}$$

Its derivative is:

$$\begin{aligned}
\dot{V}_q &= s_q \dot{s}_q \\
&= s_q \left[\bar{f}_f(q,t) + \Delta f_f + g_f(t)\delta_e(t) - \dot{q}_c + c_q(q - q_c) \right] \\
&= s_q \left[\Delta f_f - L_q - \beta_q \operatorname{sat}(s_q) \right] \\
&\le \left(\Delta f_f - L_q \right) |s_q| - \beta_q |s_q| \\
&< -\beta_q |s_q| < 0
\end{aligned} \tag{22}$$

This indicates that the system is stable under the control law in Eq. 19. Moreover, the dynamics of the system on the sliding surface can be dominated by the β_q, as $\Delta f_f - L_q$ is a small perturbation. In that case, the convergence rate of the state toward the sliding surface is:

$$\dot{s}_q \approx -\beta_q \operatorname{sat}(s_q) \tag{23}$$

Therefore, it is possible to improve the response speed and quality of the system by designing β_q without sacrificing stability. An appropriate convergence rate can reduce system chattering. The ideal convergence rate is designed such that the speed of the state point moving toward the manifold is large when far from the manifold and asymptotically zero when near it (Boiko 2008). Based on this idea, the sliding mode gain β_q is designed as:

$$\beta_q = \frac{\omega_q}{2^{\alpha_q}} |s_q|^{2\alpha_q - 1} \tag{24}$$

where ω_q is a positive gain and $\alpha_q \in (0.5, 1.0)$. They are tuned to achieve optimal trade-offs between response speed, stability margins, and control effort. The sliding mode gains were selected to satisfy the robustness condition $\beta_q > \left| \Delta f_f - L_q \right|$ while minimizing chattering.

Consequently, the control law for q loop is:

$$\delta_e = \frac{-\bar{f}_f(t) - L_\alpha - c_q(q - q_c) + \dot{q}_c - \dfrac{\omega_q}{2^{\alpha_q}} |s_q|^{2\alpha_q - 1} \operatorname{sat}(s_q)}{g_f(t)} \tag{25}$$

Sliding mode control design for α loop

The α loop dynamic equation of the folding-wing aircraft can be modeled as the following nonlinear affine system:

$$\begin{cases} \dot{\alpha} = f_s(\alpha,t) + g_s(t)q \\ y = \alpha \end{cases} \tag{26}$$

where $f_s(\alpha,t)$ is the nonlinear drift term of the angle-of-attack dynamics, and $g_s(t)$ is the input gain function of the angle-of-attack dynamics:

$$\begin{cases} f_s(\alpha,t) = \dfrac{1}{mV}[-T\sin\alpha - L + mg\cos\gamma \\ \qquad -(-S_z\dot{q} - 2q\dot{S}_z)\sin\alpha + (q^2S_z - \ddot{S}_z)\cos\alpha] \\ g_s(t) = 1 \end{cases} \tag{27}$$

According to the preceding analysis, L includes the uncertainty from unsteady aerodynamics in the wing-folding process. Rewriting the function $f_s(\alpha,t)$ to account for uncertainty:

$$f_s(\alpha,t) = \bar{f}_s(\alpha,t) + \Delta f_s \tag{28}$$

where $\bar{f}_s(\alpha,t)$ is the nominal value of $f_s(\alpha,t)$ and Δf_s is the bounded uncertainty, which meets the following bound:

$$|\Delta f_s| < L_\alpha \tag{29}$$

and L_α is a positive bound of α loop dynamics uncertainty.

Using the same method, the α loop-sliding surface s_α is chosen as:

$$s_\alpha = e + c_\alpha \int e dt \tag{30}$$

where c_α is the sliding surface slope of α loop. Its derivative is:

$$\begin{aligned} \dot{s}_\alpha &= \dot{e} + c_\alpha e \\ &= \dot{\alpha} - \dot{\alpha}_c + c_\alpha(\alpha - \alpha_c) \\ &= f_s(\alpha,t) + g_s(t)q - \dot{\alpha}_c + c_\alpha(\alpha - \alpha_c) \\ &= \bar{f}_s(\alpha,t) + \Delta f_s + g_s(t)q - \dot{\alpha}_c + c_\alpha(\alpha - \alpha_c) \end{aligned} \tag{31}$$

Employing the same feedback control law, the following expression is obtained:

$$q = \frac{-\bar{f}_s(\alpha,t) - L_\alpha - c_\alpha(\alpha - \alpha_c) + \dot{\alpha}_c - \frac{\omega_\alpha}{2^{\alpha_\alpha}}|s|^{2\alpha_\alpha - 1}\operatorname{sat}(s_\alpha)}{g_s(t)} \tag{32}$$

Proportional-integral-derivative control design for the flight-path control loop

The outer loop of the flight control system is the flight-path controller, whose dynamic response is slower than that of the inner loop and is slightly influenced by the time-varying factors. Therefore, the outer-loop controller is built based on the classic PID control method. The structure of the outer-loop controller is shown in Fig. 4, where H_c and V_c are altitude and speed command signals.

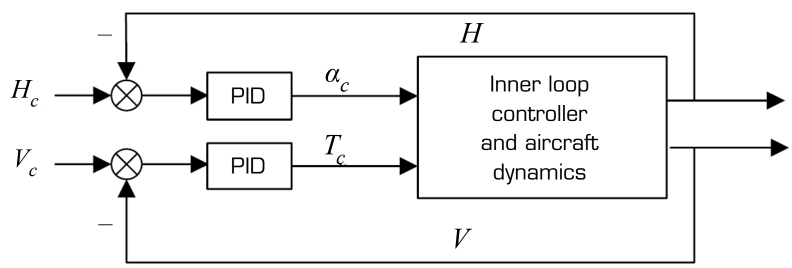

Source: Elaborated by the author.

Figure 4. Structure of the outer loop controller.

The foundation of the outer-loop controller is to generate the angle-of-attack command α and thrust command T_c according to the reference signals of altitude and speed. Thrust and the angle of attack influence the speed and altitude directly. Therefore, the transfer functions of the PID controller are:

$$\frac{\alpha_c}{e_H} = P_H + I_H \frac{1}{S} + D_H \frac{N}{1 + N\frac{1}{S}}, N = 100 \tag{33}$$

$$\frac{T_c}{e_V} = P_V + I_V \frac{1}{S} + D_V \frac{N}{1 + N\frac{1}{S}}, N = 100 \tag{34}$$

where α_c, T_c are the angle-of-attack and thrust command signals, P_H, I_H, D_H, P_V, I_V, D_V are the controller parameters to be designed, N is the coefficient of the approximate differentiator, and S is the Laplace operator.

Closed-loop simulation and verification

For the above integrated flight controller, the parameters are adjusted according to performance. The specific control system parameters are shown in Tables 3 and 4.

Table 3. SMC parameters.

ω_q	α_q	c_q	ω_α	α_α	c_α
12	0.9	1	3	0.65	0.1

Source: Elaborated by the author.

Table 4. PID parameters.

P_H	I_H	D_H	P_V	I_V	D_V
0.01	0	0.08	30	0	50

Source: Elaborated by the author.

After specifying the control parameters, the closed-loop flight simulation of the folding-wing aircraft is required to verify the effectiveness and robustness of the control system.

Simulation of the wing-folding process

Three different trim points are simulated; they are $H = 3000\text{m}$, $Ma = 0.6$; $H = 5000\text{m}$, $Ma = 0.9$ and $H = 8000\text{m}$, $Ma = 1.3$. At each trim point, the folding-wing aircraft is initially in straight-and-level flight, and its outer wing folds upward from 0° to 60°. Its dynamic response is shown in Fig. 5.

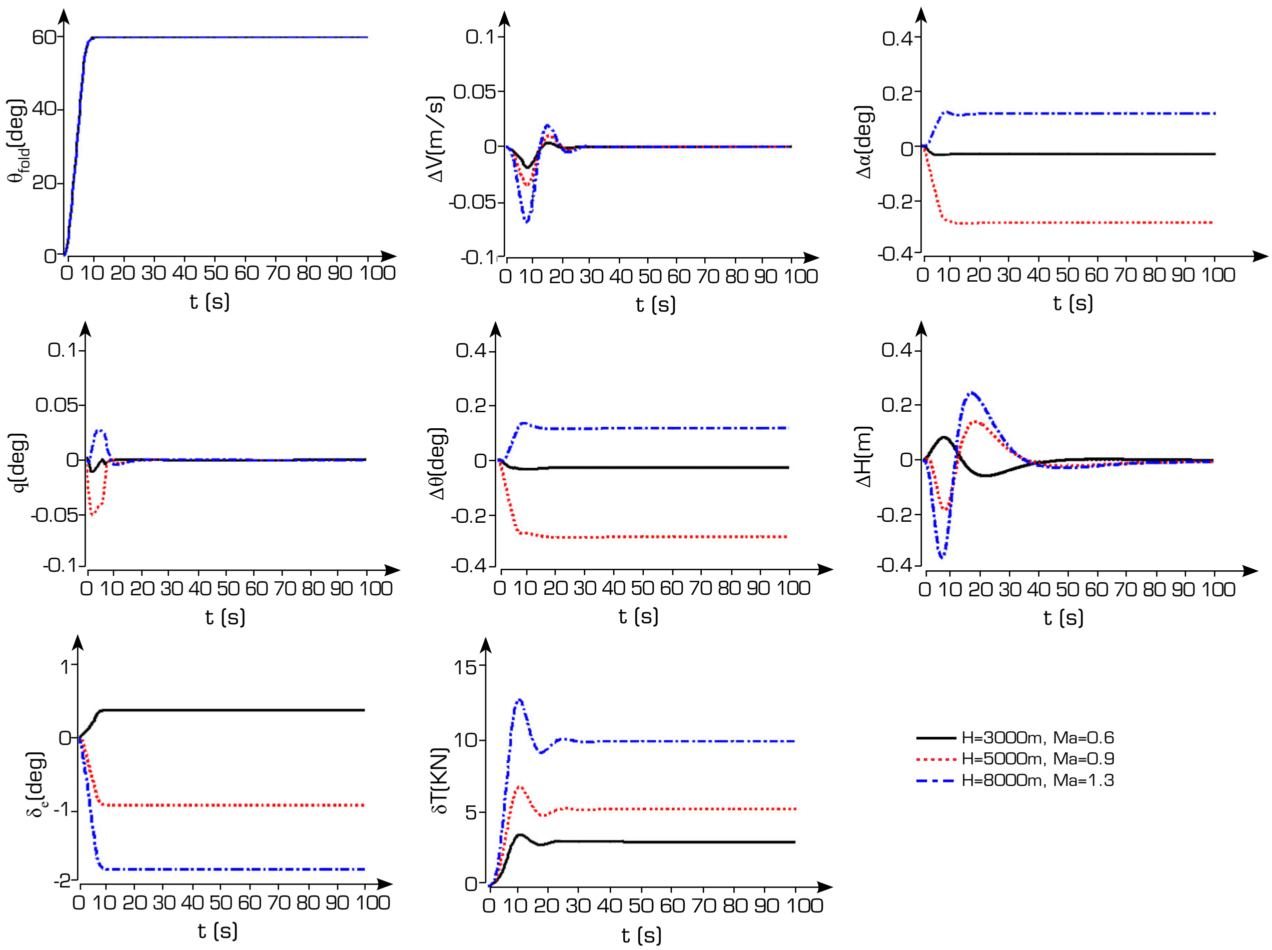

Source: Elaborated by the author.

Figure 5. Simulation result of the wing folding process.

In Fig. 5, θ_{fold} is the wing-folding angle, q is the pitch angular velocity, and $\Delta(\cdot)$ means the increment relative to the initial trim value of each flight parameter.

The results show that after the morphing phase, the flight parameters approach a stable state within a short time (10 to 30 seconds), while speed and altitude are maintained at their initial values. Consequently, the integrated flight control system guarantees the global stability of the closed-loop system during the wing-folding process. Moreover, during the morphing phase, the pitch angular velocity varies within the range of 8×10^{-2} deg·s^{-1}, the angle of attack varies within the range of 4×10^{-1} deg, and altitude and speed vary within the ranges of 6×10^{-1} m and 9×10^{-2} m·s^{-1}, respectively, which are all minor changes. Therefore, the wing-folding movement has a negligible impact on flying qualities and safety under the regulation of the flight control system. The proposed integrated controller successfully achieves its primary objective: a smooth and stable transition from the unfolded to the folded configuration.

Verification of the robustness of the control system

As the effect of unsteady aerodynamics during the wing-folding process is ignored, the multibody dynamic model contains uncertainty. This uncertainty is represented by adding parameter perturbations when verifying the robustness of the control system. It is assumed that the perturbations of the force and torque coefficients are as follows.

$$\begin{cases} C_L' = \left(0.8 - 0.5\dfrac{\pi}{180}\alpha^\circ\right)C_L \\ C_D' = \left(1.2 + 0.5\dfrac{\pi}{180}\alpha^\circ\right)C_D \\ C_m' = \left(0.8 - 0.5\dfrac{\pi}{180}\alpha^\circ\right)C_m \end{cases} \tag{35}$$

where C' is the perturbation value and C is the nominal value.

The same simulation is run at the trim point $H = 8000$ m, $Ma = 1.3$. The results are shown in Fig. 6.

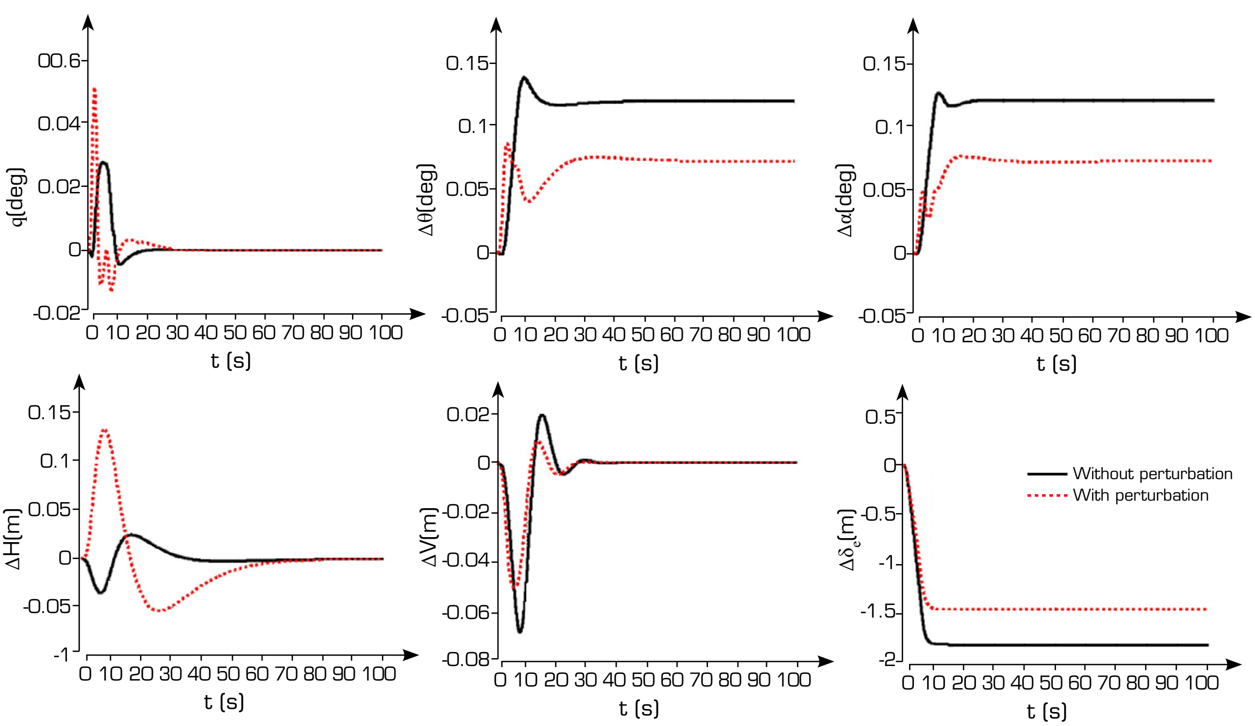

Source: Elaborated by the author.

Figure 6. Simulation result of robustness verification.

In the presence of aerodynamic parameter perturbations, the integrated control system guarantees the stability of the closed-loop system during the wing-folding process. The response of the flight parameters is nearly identical to that with nominal parameters and reaches a steady state in finite time. This robustness verification conclusively demonstrates that the hybrid SMC-PID architecture effectively compensates for model uncertainties, fulfilling the core robustness requirement for practical morphing aircraft control.

CONCLUSION

This paper develops an SMC algorithm for folding-wing aircraft to address the modeling uncertainty arising from unsteady aerodynamics during the wing-folding process. A nonlinear dynamic model of the aircraft is established using Newtonian mechanics, accounting for multibody dynamics, shifting CG, and time-varying aerodynamic characteristics. Based on time-scale separation, the integrated flight control system is partitioned into inner (fast) and outer (slow) control loops, allowing sliding mode control and PID control to be applied to each layer, respectively. The principal contribution of this work is the novel integration of these two control paradigms into a single, cohesive framework specifically designed for the unique challenges of large-scale morphing.

Closed-loop simulations demonstrate that the proposed integrated flight controller effectively ensures a smooth transition of the folding-wing aircraft from the unfolded to the folded configuration while maintaining the required robustness of the flight control system. Specifically, simulation results show that during the wing folding process:

- Altitude regulation error is maintained within ± 1.0 m under nominal conditions and ± 1.5 m under perturbed conditions
- Velocity regulation error is kept within ± 0.1 $m \cdot s^{-1}$ under nominal conditions and ± 1.8 $m \cdot s^{-1}$ under perturbed conditions.
- Pitch-rate variations are bounded by ± 0.03 $deg \cdot s^{-1}$ under nominal conditions and ± 0.06 $deg \cdot s^{-1}$ under perturbed conditions.
- Attitude settling time after morphing completion is less than 25 seconds, and altitude settling time is less than 50 seconds across all tested trim conditions.

The controller demonstrates robustness to ± 20% aerodynamic coefficient uncertainties with less than 25% degradation in regulation performance.

The switching gain design in the SMC effectively reduces chattering while maintaining robustness. The PID outer loop successfully regulates flight-path variables, with steady-state errors approaching zero due to integral action. This work provides a practical and theoretically sound solution that paves the way for the real-world implementation of advanced folding-wing aircraft.

CONFLICTS OF INTEREST

Nothing to declare.

DATA AVAILABILITY STATEMENT

The data will be available upon request.

FUNDING

No funding.

DECLARATION OF USE OF ARTIFICIAL INTELLIGENCE TOOLS

The author utilized DeepL to assist with the translation and linguistic polishing of the original manuscript. The author confirms that the scientific content and logic remain unchanged and accepts full accountability for the final text.

ACKNOWLEDGEMENTS

Not applicable.

REFERENCES

Apkarian P, Gahinet P, Becker G (1995) Self-scheduled H∞ control of linear parameter-varying systems: a design example. Automatica 31(9):1251-1261. https://doi.org/10.1016/0005-1098(95)00038-X

Bai X, Xing X, Liu L, Zhang J, Ling C, Li Z (2020) Design of a trans-media aircraft morphing wing structure. Paper presented 2020 2nd International Conference on Artificial Intelligence and Advanced Manufacture. IEEE; Shanghai, China. https://doi.org/10.1109/AIAM50918.2020.00013

Boiko IM (2008) Extension of harmonic balance principle and its application to analysis of convergence rate of second-order sliding mode control algorithms. American Control Conference. IEEE, Seattle, USA. https://doi.org/10.1109/ACC.2008.4587235

Dai P, Yan B, Liu R, Liu S, Wang M (2021) Integrated morphing strategy and trajectory optimization of a morphing waverider and its online implementation based on the neural network. IEEE Access 9:59383-59393. https://doi.org/10.1109/ACCESS.2021.3073207

Khalil HK (2008) Nonlinear systems Third Edition. Englewood Cliffs; Prentice Hall. [accessed Jun10 2026]. https://api.semanticscholar.org/CorpusID:59790953

Kocamer A, Kose O, Şal F, Oktay T (2025) Conceptual design of simultaneous wing dihedral adjustment and control system for a mini VTOL UAV. Aircr Eng Aerosp Technol 97(9):1149-1158. https://doi.org/10.1108/AEAT-11-2024-0313

Kose O, Oktay T, Özen E (2023) Simultaneous arm morphing quadcopter and autonomous flight system design. Aircr Eng Aerosp Technol 95(10):1624-1632. https://doi.org/10.1108/AEAT-05-2023-0146

Liu S, Yan B, Dai P, Xing M (2019) Morphing aircraft control method based on T-S fuzzy control. Paper presented 2019 IEEE 4th International Conference on Image, Vision and Computing. IEEE; Xiamen, China. https://doi.org/10.1109/ICIVC47709.2019.8980976

Moorhouse D, Sanders B, von Spakovsky MR, Butt J (2006) Benefits and design challenges of adaptive structures for morphing aircraft. Aeronaut J 110(1105):157-162. https://doi.org/10.1017/S0001924000001135

Nie L, Zhou M (2021) Adaptive output feedback dynamic surface sliding mode control for a class of uncertain nonlinear systems with unknown actuator hysteresis. Paper presented 2021 IEEE 7th International Conference on Control Science and Systems Engineering. IEEE; Qingdao, China. https://doi.org/10.1109/ICCSSE52761.2021.9545176

Oktay T (2014) Performance of minimum energy controllers on tiltrotor aircraft. Aircr Eng Aerosp Technol 86(5):361-374. https://doi.org/10.1108/AEAT-11-2012-0225

Oktay T, Sultan C (2014) Flight control energy saving via helicopter rotor active morphing. J Aircr 52(3):843-855. https://doi.org/10.2514/1.C032494

Özgür B, Sahin H, Oktay T (2025) Combined autopilot, powerplant and vertical tail redesign for best performance of TUAV. Aircr Eng Aerosp Technol 97(10):1300-1310. https://doi.org/10.1108/AEAT-03-2025-0103

Peng W, Yang T, Feng Z, Zhang Q (2019) Analysis of morphing modes of hypersonic morphing aircraft and multiobjective trajectory optimization. IEEE Access 7:2244-2255. https://doi.org/10.1109/ACCESS.2018.2886252

Shabana AA (2020) Dynamics of multibody systems. 5th ed. Cambridge: Cambridge University Press. https://doi.org/10.1017/9781108757553

Takarics B, Mocsányi RD, Vanek B, Sziroczák D, Rohács D (2020) Aerodynamic and LPV modeling of a distributed propulsion morphing wing aircraft. Paper presented 2020 2nd IEEE International Conference on Gridding and Polytope Based Modelling and Control. IEEE; Budapest, Hungary. https://doi.org/10.1109/GPMC50267.2020.9333823

Umar A, 2025. Robust Backstepping Sliding Mode Control for a Morphing Quadcopter UAV. Engineering Proceedings, 87. https://doi.org/10.3390/engproc2025087086

Wu CF, Shao PY, Ma SH (2013) An effective design of LPV based robust gain-scheduling controller for morphing-wing UAV. Paper presented 32nd Chinese Control Conference. TCCT; Xi'an, China. [accessed Jun10 2026]. https://ieeexplore.ieee.org/document/6639874

Yesilbas E, Özgür B, Ozen E, Oktay T (2025) Simultaneous and stochastic design of piston-prop TUAV vertical tail and its autonomous system. Aircr Eng Aerosp Technol 97(4):395-404. https://doi.org/10.1108/AEAT-11-2024-0311

Yue T, Wang L (2013) Longitudinal linear parameter varying modeling and simulation of morphing aircraft. J Aircr 50(6). https://doi.org/10.2514/1.C031316

Zhen H, Yingying K, Da L (2017) Deep stall landing strategy for small fixed-wing aircraft aided by morphing. Paper presented 2017 29th Chinese Control and Decision Conference. IEEE; Chongqing, China. https://doi.org/10.1109/CCDC.2017.7978398

Zhu L, Liu Z, Li L (2017) Modeling and aerodynamic characteristics analysis of morphing aircraft. Paper presented 2017 29th Chinese Control and Decision Conference. IEEE; Chongqing, China. https://doi.org/10.1109/CCDC.2017.7978791